Geophysical Journal International

Geophys. J. Int. (2012) **190,** 913–921 doi: 10.1111/j.1365-246X.2012.05525.x

GPS studies of active deformation in the Pyrenees

E. Asensio,[1] G. Khazaradze,[1] A. Echeverria,[1] R. W. King[2] and I. Vilajosana[3]

[1] *Departament de Geodinàmica i Geofísica, Facultat de Geologia, Universitat de Barcelona* 08028*, Barcelona, Spain. E-mail: evasensio@ub.edu*
[2] *Departament of Earth, Atmospheric and Planetary Sciences, Massachusetts Institute of Technology, Cambridge, MA* 02139*, USA.*
[3] *WorldSensing, Barcelona* 08023*, Spain*

Accepted 2012 April 23. Received 2012 April 23; in original form 2011 July 08

SUMMARY

The Pyrenees mountain belt, which separates the Iberian Peninsula from the rest of the European continent, is part of the Alpine–Himalayan orogenic belt, formed as a result of a collision between the African and Eurasian Plates. Although the instrumental seismicity in the Pyrenees is moderate, in the past centuries a number of destructive earthquakes have occurred, which could indicate continuing tectonic activity of the area. We analyse GPS observations spanning 3.5 yr from 35 continuous stations in the Pyrenees region and find significant ongoing extension perpendicular to the range at 2.5 ± 0.5 nstrain yr^{-1}, with the possibility of higher strain rates concentrated in the westernmost part of the range. This finding is in agreement with the predominantly normal faulting focal mechanisms of earthquakes that occur in the area and suggests a recurrence time for magnitude 6.5 earthquakes of 2200–2500 yr.

Key words: Time series analysis; Satellite geodesy; Seismicity and tectonics; Continental tectonics: extensional; Europe.

1 INTRODUCTION

The Pyrenees mountain range separates the Iberian Peninsula from the rest of Europe and is part of the Alpine–Himalayan orogenic belt. The geologic evolution of the range was dominated by two major events; an extensional episode during the middle and late Cretaceous related to the opening of the Bay of Biscay, followed by a compressive episode during the late Cretaceous to earliest Miocene due to the collision of the Iberian and Eurasian Plates (Choukroune 1992; Vergés *et al.* 2002).

The geology and structural features of the Pyrenees present a doubly-vergent orogen (e.g. Teixell 1996) differentiated into several parts (Fig. 1): a northern belt, denoted as the North-Pyrenean Zone (NPZ), where folds and thrusts face towards the Aquitanian foreland basin, to the north and a southern belt, characterized by South-vergent folds and thrusts, facing towards the Ebro foreland basin, to the south. The southern belt also includes an Axial Zone formed by Hercynian basement rocks.

The Axial Zone and the NPZ are separated by a North Pyrenean Fault (NPF) which represents a suture between the Eurasian and Iberian Plates. This fault is not clearly identified at the surface, but is inferred at depth from the related Moho offset (Gallart *et al.* 1985). Most of the instrumentally recorded earthquakes are associated with this fault (Souriau & Pauchet 1998), especially in the western part of the range (Fig. 2).

Except for the observed seismicity, no direct evidence exists to characterize present-day tectonic activity of the NPF or other faults in the Pyrenees. The main goal of the presented work is to determine whether any tectonic motions can be detected using high-precision GPS geodesy. The answer to this question is important for the advancement of our knowledge of the tectonics of the mountain range, as well as for better evaluation of the regional seismic hazard. We analyse data from all available continuous GPS stations (CGPS) in operation since 2008 to estimate relative velocities and their uncertainties. We use these velocities to constrain the strain rate across the range and find significant range-normal extension consistent with earthquake focal mechanisms. From observed strain rates, we estimate the repeat time for the 'maximum credible earthquake' (MCE; M_w6.5) for the Pyrenees.

2 PREVIOUS STUDIES

2.1 Instrumental and historical seismicity, focal mechanisms and stress

The instrumental seismicity in the Pyrenees is moderate. According to the NEIC catalogue (neic.usgs.gov), from 1973 to 2011, more than ∼3500 earthquakes with M >2 occurred in and around the Pyrenees (Fig. 2). 75 per cent of these events have magnitudes between 2 and 3; 23 per cent between 3 and 4; and 2 per cent between 4 and 5. Only four earthquakes have magnitudes ≥5 and these are mainly concentrated in the Lourdes area in France. These events are related to the east–west oriented Cretaceous faults that form part of the North Pyrenean Frontal thrust (Gagnepain-Beyneix *et al.* 1982; Sylvander *et al.* 2008).

The seismicity is mainly concentrated in the western part of the NPF (Souriau & Pauchet 1998). The eastern region is characterized by lower and more diffuse seismicity related to the Mediterranean System, which includes the Catalan Coastal Range (CCR)

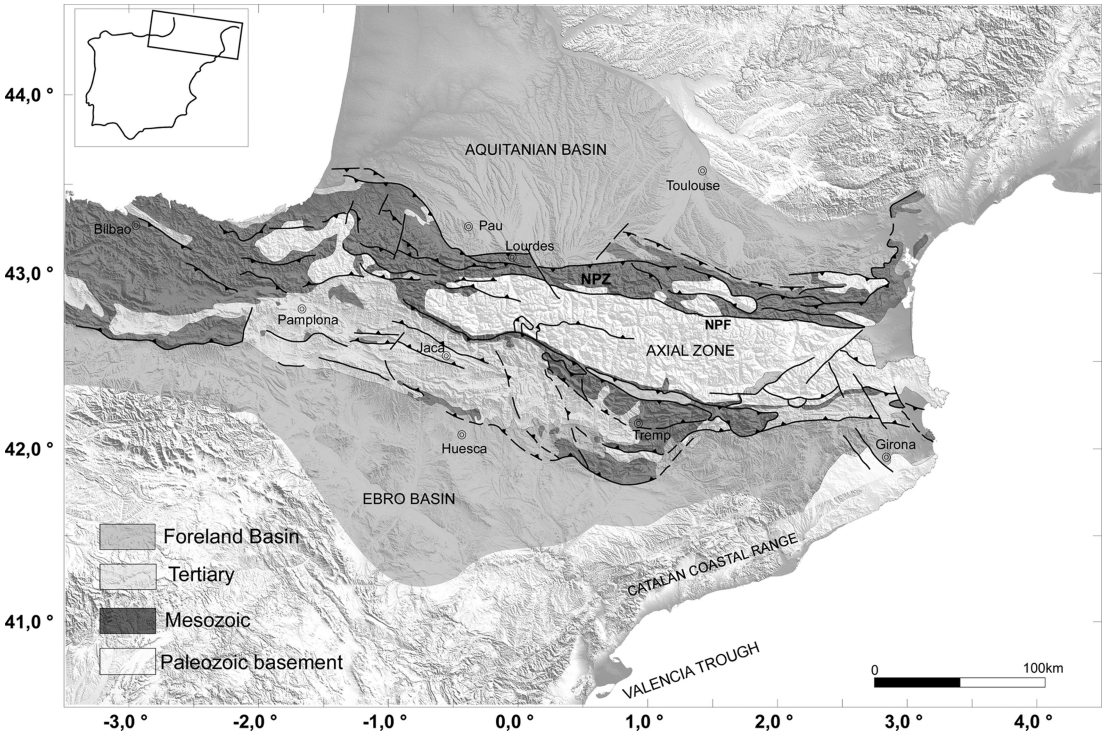

Figure 1. Geologic map of the Pyrenees. NPF, North Pyrenean Fault; NPZ, North Pyrenean Zone. The inset shows the location of the study area within the Iberian Peninsula. Figure modified from Teixell (1996).

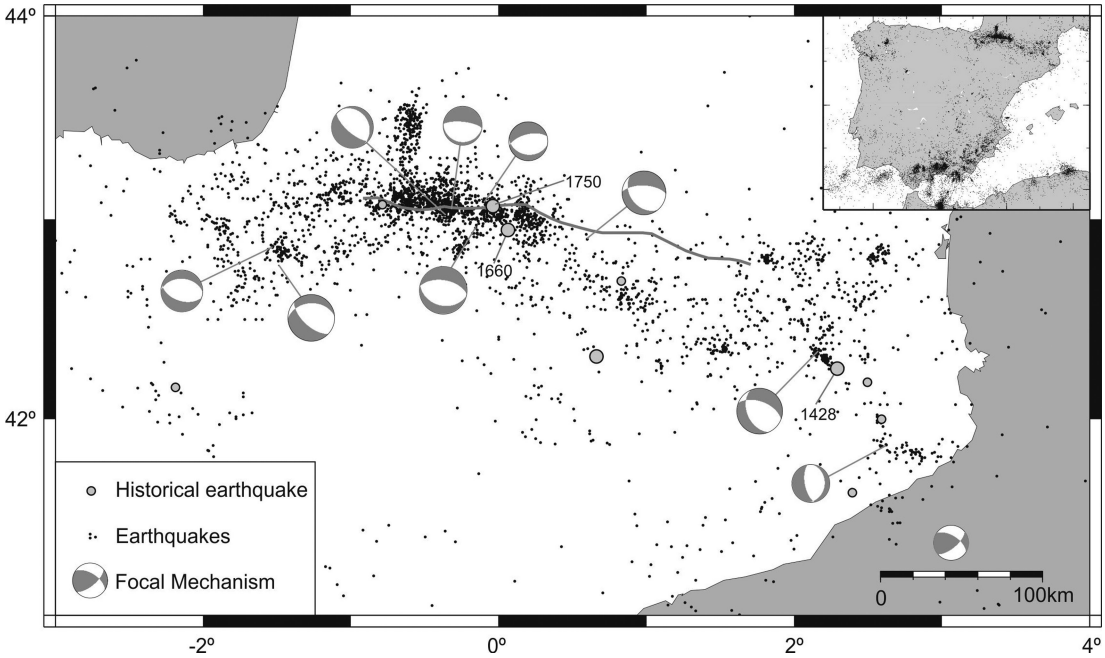

Figure 2. Seismicity map of the Pyrenees and the entire Iberian Peninsula (the inset) during the 1973–2011 time period. Earthquakes with $M > 2$ were chosen from the USGS/NEIC catalogue (http://neic.usgs.gov). Grey dots depict historical earthquakes of MSK $\geq$VIII (Olivera *et al.* 2006; Souriau & Pauchet 1998). Focal mechanisms (1984–2008) are from Stich *et al.* (2006, 2010). Grey line depicts the North Pyrenean Fault (NPF).

and the Valencia Trough (Banda & Santanach 1992; Roca *et al.* 1999; Fig. 1). The earthquakes are generally shallow, not exceeding 20 km depth, which suggests an average thickness for the seismogenic crust of ∼15 km (Perea 2009).

The focal mechanisms displayed in Fig. 2 were obtained by Stich *et al.* (2006, 2010) using moment tensor inversion for regional earthquakes higher than M_w3.5 from 1986 to 2008. They calculated 10 focal mechanisms, with eight events falling within the region of our study and two in the CCR. All of the Pyrenees earthquakes indicate normal faulting with approximately NNE–SSW oriented tension axes, roughly perpendicular to the trend of the mountain chain. The two focal mechanisms outside the Pyrenees show a different stress regime (Fig. 2): strike slip and east–west extension.

On the other hand, the compilation of focal mechanisms given by Goula *et al.* (1999) provide a more complex seismotectonic picture for the Pyrenees, specifically for the eastern part, where the authors determined the seismic and microtectonic stress fields using seismic focal mechanisms and striation measurements, respectively. The microtectonic study of 23 sites shows a relatively homogeneous north–south direction of the maximum horizontal stress (σ_1) with interplay between the intermediate (σ_2) and minimum (σ_3) stress directions from vertical to east–west, indicating strike-slip and compressive regimes, respectively. The seismic stress orientations deduced from a compilation of 18 focal mechanisms obtained by various authors using mainly first *P*-arrivals (see Fig. 4 on page 495 and accompanying Table 2 on page 496 of Goula *et al.* (1999) for more details), showed 15.5 strike-slip and 2.5 reverse fault earthquakes, where the events with two possible solutions counted as a half unit. The deduced orientation of maximum horizontal stress (σ_1) is also approximately north–south.

Another study of earthquake focal mechanisms in the Iberian Peninsula that included earthquakes in the Pyrenees was conducted by Herraiz *et al.* (2000). The authors analysed 22 earthquakes from 1980 to 1996 with $M_w > 3.3$ for the Pyrenees. Although the estimated stress orientations are complex, for the western part of the chain, where most of the earthquakes are concentrated (Fig. 2), the maximum horizontal stress (σ_1) indicates north–south compression, similar to the results of Goula *et al.* (1999) obtained for the eastern part, but opposite to the focal mechanisms computed by Stich *et al.* (2006).

The most recent relevant studies of the stress regime in the Pyrenees include papers by Olaiz *et al.* (2009) and De Vicente *et al.* (2008), who developed a strain–stress map of Europe and Iberia, respectively. The maps were obtained from the direct inversion of compilations of earthquake focal mechanisms from various sources. For the Pyrenees area, most of the focal mechanisms used by the authors come from Stich *et al.* (2006), thus it is not surprising that their maximum horizontal stress (σ_1) indicates extension in the direction of ∼NE–SW, which the authors attribute to normal readjustments or post-orogenic topographic compensation (Caputo *et al.* 1984).

Since 1373, there have been 10 significant earthquakes (with intensity higher than VIII) in the Pyrenees: four events with MSK Intensity of IX (roughly equivalent to 6.5 magnitude event) and six with MSK of VIII (Souriau & Pauchet 1998; Olivera *et al.* 2006; Perea 2009). The most destructive of these occurred on 1428 February 2 near the village of Camprodon in the eastern Pyrenees, causing the deaths of 1000 people (Fig. 2). This earthquake formed part of the Catalan seismic crisis of 1427–1428 (Figueras *et al.* 2006). Two other significant earthquakes took place in 1660 and 1750 in the Lourdes area in France where, as mentioned earlier, the strongest instrumentally recorded earthquakes have occurred.

2.2 Previous deformation studies

Since 1992, two GPS projects have been developed in the Pyrenees area with the objective of quantifying crustal deformation rates. The PotSis network (Goula *et al.* 1996) in the eastern Pyrenees was surveyed in 1992, 1994, 1999 (Térmens *et al.* 2000) and 2006. Preliminary results based on the first three surveys were presented by Talaya *et al.* (1999) and Khazaradze *et al.* (2004), but no statistically significant velocities were obtained. The ResPyr network (Fleta *et al.* 1996) covers the whole area of the Pyrenees and was surveyed in 1995, 1997 and 2008. Unfortunately, during the first two surveys, only half of the network was observed. The first preliminary results presented by Chenel *et al.* (2009) of the ResPyr network indicate no significant deformation in the Pyrenees.

Other studies have used CGPS throughout Europe, including a small number on each side of the Pyrenees, to estimate the relative motion between Eurasia and Iberia. Nocquet & Calais (2003) analysed data from 1996 to 2006 for sites with a minimum of 2 yr of observations. Based largely on the results for three well-determined stations in Spain, they concluded that an upper bound for the active motion across the Pyrenees is approximately 0.6 mm yr^{-1}. Fernandes *et al.* (2007) analysed data from 1996 to 2005 for stations observing for at least 3.5 yr and concluded that any differential motion between Iberia and Eurasia cannot be detected at the level of 0.85 mm yr^{-1}. The GPS studies of Serpelloni *et al.* (2007) and Stich *et al.* (2006) both used data from 1998 to 2005, but included only two and five stations, respectively, within our research area. Their results for the Pyrenees are again non-conclusive. However, Stich *et al.* (2006) do suggest a possibility of a slight S–SE motion of the Iberian stations with respect to Eurasia, which could be indicative for an ongoing extension in the Pyrenees although they provide no upper or lower bound.

Geologic studies that can be compared with the GPS results are scarce. Apart of the previously mentioned study of the stress field by Goula *et al.* (1999), there are several other geologic studies of various faults in the area, mainly providing estimates for the relative vertical slip rates (Briais *et al.* 1990; Fleta *et al.* 2001; Masana *et al.* 2001; Perea *et al.* 2003; Alasset & Meghraoui 2005; Ortuño *et al.* 2008). As a consequence, although these studies provide evidence of fault motion with maximum vertical geologic slip rates of 0.3 mm yr^{-1}, a direct comparison with the GPS horizontal velocities is not straightforward. In theory, a methodology exists to establish a relation between the two, taking into account fault geometry and specifically its dip angle (e.g. Niemi *et al.* 2004), but the regional character of the GPS studies, high errors associated with the geologic slip rates and the very distinct time ranges (the geologic slip rate cover 1–20 Ma) render a comparison not useful.

3 GPS OBSERVATIONS AND ANALYSIS

3.1 GPS data

We processed data from 35 CGPS belonging to various GPS networks operating in the Pyrenees, covering a 3.5-yr time period from 2008 March to 2011 August. Although data from up to 7 yr are available for some stations, in order to minimize the effects on our strain estimates of spatially and temporally correlated errors (see Sections 3.3 and 5.1 below), we included in our analysis data from all stations for nearly the same time span. We chose 3.5 yr since that is close to the maximum span available for the western Pyrenees stations and corresponds to one of the spans for which annual signals have minimal effect on velocity estimates (Blewitt & Lavallée 2002). The majority of the data come from regional networks in Spain and France: CATNET in Catalonia (Talaya *et al.* 2000), RGAN in Navarra (www.navarra.es/appsext/rgan), Topo-Iberia (Garate *et al.* 2008) in Spain and the RGP network in France (Duquesnoy 2003). We have also included in our analysis data from CGPS sites located outside the study area (see Table 1) in order to define a stable reference frame for assessing deformation within the Pyrenees. The bulk of the data from these additional stations come from the International GPS Service (IGS) for Geodynamics (Beutler *et al.* 2008), European Permanent (EPN-EUREF)

Table 1. Horizontal velocities and 1σ uncertainties of the stations included in our solution. Velocities are in the western Europe reference frame defined by the seven stations shown with an asterisk (*). V_e is the east component, V_n, the north component, V_h the horizontal magnitude, Az the azimuth and ρ is a correlation coefficient between the east and north components; sites used to maintain the reference frame for generation of time-series are in bold; Pyrenees sites are the first 35 sites, other IGS sites used are from 36 to 49. Velocities of the two stations at Toulouse (TLMF and TLSE stations) are linked in the estimation.

#	ID	Latitude	Longitude	$V_e \pm 1\sigma$		$V_n \pm 1\sigma$		$V_h \pm 1\sigma$		ρ	Az
1	ALSA	38°20′20″ N	02°85′20″ W	−1.03	0.17	−0.18	0.17	1.05	0.17	0.005	255
2	ASIN	42°30′59″ N	00°05′54″ W	−0.32	0.19	−0.83	0.20	0.89	0.20	0.004	202
3	**AUCH**	**43°38′58″ N**	**00°34′50″ E**	**0.85**	**0.37**	**−0.93**	**0.33**	**1.26**	**0.35**	**0.008**	**142**
4	AVEL	41°52′53″ N	00°45′11″ E	0.23	0.71	−1.98	0.73	1.99	0.73	0.002	175
5	**BARY**	**43°02′08″ N**	**00°40′18″ E**	**−0.43**	**0.24**	**−0.50**	**0.24**	**0.66**	**0.24**	**0.007**	**219**
6	**BELL**	**41°35′58″ N**	**01°24′04″ E**	**−0.31**	**0.20**	**−0.23**	**0.21**	**0.39**	**0.20**	**0.004**	**227**
7	**BIAZ**	**43°28′19″ N**	**01°32′12″ W**	**0.19**	**0.22**	**−0.61**	**0.21**	**0.64**	**0.21**	**0.010**	**169**
8	CASS	41°52′58″ N	02°54′15″ E	0.01	0.33	0.10	0.21	0.10	0.21	0.004	270
9	CREU	42°19′07″ N	03°18′56″ E	−0.03	0.16	−0.89	0.16	0.89	0.16	0.007	185
10	**EBRE**	**40°49′15″ N**	**00°29′32″ E**	**−0.18**	**0.15**	**−1.07**	**0.21**	**1.09**	**0.21**	**0.009**	**191**
11	**EPSH**	**42°07′08″ N**	**00°26′53″ W**	**−0.03**	**0.34**	**−1.01**	**0.40**	**1.01**	**0.40**	**0.003**	**184**
12	ESCO	42°41′36″ N	00°58′32″ E	−0.28	0.19	−0.57	0.16	0.64	0.17	0.004	207
13	**FJCP**	**43°02′53″ N**	**02°47′41″ E**	**−0.44**	**0.16**	**−0.55**	**0.16**	**0.70**	**0.16**	**0.003**	**217**
14	**FUEN**	**42°21′36″ N**	**0°53′06″ W**	**−0.17**	**0.15**	**−0.89**	**0.15**	**0.91**	**0.15**	**0.009**	**193**
15	**GARR**	**41°17′34″ N**	**01°54′50″ E**	**−0.26**	**0.16**	**−0.30**	**0.16**	**0.40**	**0.16**	**0.009**	**217**
16	**LLIV**	**42°28′41″ N**	**01°58′22″ E**	**−0.02**	**0.15**	**−0.38**	**0.18**	**0.38**	**0.18**	**0.005**	**188**
17	LNDA	42°57′36″ N	02°34′40″ W	−0.28	0.17	−0.40	0.18	0.49	0.18	0.006	214
18	LOSA	42°34′04″ N	02°11′42″ W	−0.44	0.15	−0.70	0.18	0.83	0.17	0.006	212
19	MATA	41°32′23″ N	02°25′43″ E	−0.24	0.19	−0.53	0.19	0.58	0.19	0.009	205
20	**MIMZ***	**44°12′02″ N**	**01°13′41″ W**	**0.00**	**0.20**	**−0.20**	**0.23**	**0.20**	**0.23**	**0.007**	**188**
21	**MSGT**	**42°52′46″ N**	**01°37′45″ E**	**−0.06**	**0.27**	**−0.13**	**0.23**	**0.14**	**0.24**	**0.007**	**208**
22	MTDM	43°52′57″ N	00°29′05″ W	−0.25	0.30	−0.69	0.24	0.73	0.25	0.009	201
23	**ORON**	**43°08′21″ N**	**01°36′31″ W**	**−0.15**	**0.15**	**−0.82**	**0.20**	**0.83**	**0.20**	**0.005**	**192**
24	PAMP	42°48′21″ N	01°38′10″ W	−0.45	0.16	−0.90	0.18	1.01	0.18	0.006	206
25	PERP	42°41′20″ N	02°52′55″ E	−0.10	0.99	−0.51	0.52	0.52	0.55	0.002	195
26	SANG	42°34′46″ N	01°17′13″ W	−0.48	0.16	−1.81	0.30	1.87	0.29	0.004	196
27	**SBAR**	**41°58′48″ N**	**02°10′27″ E**	**0.16**	**0.15**	**−1.20**	**0.17**	**1.21**	**0.17**	**0.007**	**175**
28	SCOA	43°23′42″ N	01°40′54″ W	−0.04	0.35	−1.45	0.33	1.45	0.33	0.006	183
29	**SORI**	**42°22′28″ N**	**01°07′57″ E**	**0.09**	**0.15**	**−0.93**	**0.16**	**0.93**	**0.16**	**0.006**	**178**
30	TAFA	42°31′15″ N	01°40′36″ W	−0.42	0.15	−1.05	0.16	1.13	0.16	0.006	202
31	TLMF	43°34′28″ N	01°22′30″ E	−0.31	0.17	−0.34	0.13	0.46	0.15	0.003	213
32	**TLSE***	**43°33′38″ N**	**01°28′50″ E**	**−0.31**	**0.17**	**−0.34**	**0.13**	**0.46**	**0.15**	**0.003**	**213**
33	TUDE	42°02′54″ N	01°36′12″ W	−0.30	0.16	−1.35	0.17	1.38	0.17	0.006	194
34	**UNME**	**43°19′17″ N**	**00°19′32″ W**	**0.06**	**0.25**	**−0.60**	**0.27**	**0.60**	**0.27**	**0.008**	**179**
35	ZARA	41°38′00″ N	00°52′55″ W	−0.35	0.14	−0.88	0.15	0.95	0.15	0.012	205
36	**BOR1**	**52°06′01″ N**	**17°04′00″ E**	**0.63**	**0.17**	**0.24**	**0.28**	**0.67**	**0.21**	**0.232**	**77**
37	**BRUS***	**50°47′52″ N**	**04°21′33″ E**	**0.39**	**0.19**	**0.48**	**0.24**	**0.62**	**0.22**	**0.032**	**43**
38	**CAGL**	**39°08′09″ N**	**08°58′22″ E**	**−0.01**	**0.18**	**−0.08**	**0.16**	**0.08**	**0.16**	**−0.009**	**203**
39	**GRAS***	**43°45′16″ N**	**06°55′14″ E**	**0.12**	**0.15**	**−0.01**	**0.26**	**0.12**	**0.15**	**0.010**	**150**
40	**HERS***	**50°52′02″ N**	**00°20′10″ E**	**−0.18**	**0.18**	**0.27**	**0.26**	**0.32**	**0.24**	**−0.005**	**311**
41	**KOSG***	**52°10′42″ N**	**05°48′34″ E**	**0.00**	**0.17**	**0.19**	**0.20**	**0.19**	**0.20**	**0.053**	**333**
42	**LAGO**	**37°05′56″ N**	**08°40′06″ W**	**−1.82**	**0.31**	**0.02**	**0.23**	**1.82**	**0.31**	**0.077**	**268**
43	**MARS***	**43°16′43″ N**	**05°21′13″ E**	**0.00**	**0.17**	**0.00**	**0.18**	**0.00**	**0.18**	**0.007**	**–**
44	**POTS**	**52°22′48″ N**	**13°04′12″ E**	**0.67**	**0.21**	**1.22**	**0.38**	**1.39**	**0.35**	**−0.017**	**29**
45	**RABT**	**33°59′53″ N**	**06°51′15″ W**	**−3.82**	**0.15**	**0.38**	**0.16**	**3.84**	**0.15**	**0.117**	**274**
46	**SFER**	**36°27′51″ N**	**06°12′20″ W**	**−3.75**	**0.15**	**−0.36**	**0.15**	**3.77**	**0.15**	**0.081**	**263**
47	**VILL**	**40°26′36″ N**	**03°57′07″ W**	**−1.04**	**0.20**	**−1.05**	**0.21**	**1.48**	**0.21**	**0.027**	**224**
48	**WTZR**	**49°08′39″ N**	**12°52′44″ E**	**0.85**	**0.28**	**1.15**	**0.45**	**1.43**	**0.40**	**−0.004**	**37**
49	**ZIMM**	**46°52′37″ N**	**07°27′55″ E**	**0.15**	**0.15**	**0.60**	**0.18**	**0.62**	**0.18**	**0.031**	**10**

(Bruyninx *et al.* 2001) and Instituto Geografico Nacional (IGN) (www.01.ign.es/ign/layout/datosGeodesicos.do) networks.

3.2 Data analysis

We analysed the GPS data with the GAMIT/GLOBK software (Herring *et al.* 2010; www-gpsg.mit.edu) using the three step approach described by McClusky *et al.* (2000). Previous to these steps, we performed a quality check of the stations, which included the examination of their monumentation, availability of the uninterrupted data and the presence of correct information regarding antenna and other hardware changes from the station logs.

In the first step of our data analysis, we used daily doubly differenced GPS phase observations to estimate station coordinates together with zenith delays of the atmosphere at each station and

orbital and Earth orientation parameters (EOP). In this step we used moderate (5–10 cm) constraints to assist resolution of phase ambiguities before loosening the constraints for combination of the parameters estimates in subsequent steps. In the second step, we generated time-series in a consistent reference frame by minimizing on each day for a selected set of stations (Table 1) the difference between their estimated positions and positions implied by their coordinates (position and velocity) in the International Terrestrial Reference Frame 2008 (Altamimi *et al.* 2011), while allowing for a translation and rotation of the solution (see, e.g. Dong *et al.* 1998). To obtain clean time-series, we allowed an offset to be estimated for any discontinuities caused by antenna changes and we removed any position estimate whose uncertainty was greater than 20 mm or whose value differed by more than 10 mm from the best-fitting linear trend. In the final step of our analysis, we combined all of the data to estimate a consistent set of positions and velocities.

3.3 Error model

Given the small strain rates we expect for the Pyrenees region, a rigorous estimation of velocity uncertainties is especially important. Time-series of position estimates for our stations (Fig. 3 and Supporting Information) make clear that much of the noise in GPS observations is not random, but rather includes temporal correlations, over periods from weeks to months, often with strong seasonal signals. Previous studies of CGPS time-series (e.g. Williams *et al.* 2004) have shown that the error spectrum for most stations can be represented by a combination of seasonal signal, white noise and flicker noise. One approach to determining realistic uncertainties is to perform a spectral analysis of the time-series in which these three components are estimated. A disadvantage of this approach is that the flicker noise component cannot be included directly in our velocity solution, performed with a Kalman filter that accepts only first-order Gauss–Markov processes. Herring (2003) has proposed an alternative approach which can be incorporated directly into GLOBK and is also more computationally efficient. His 'realistic sigma' (RS) algorithm uses the fact that in the presence of correlated noise, χ^2/dof of the time-series as a function of averaging time does not remain constant (as with white noise) but increases asymptotically, as would be expected from a first-order Gauss–Markov process. By estimating the amplitude and time constant of the exponential function and then evaluating the function for infinite averaging time, we can determine the value of a random walk that will produce a realistic uncertainty for the velocity estimate (see Reilinger *et al.* 2006 or Shen *et al.* 2011 for details). We applied the RS algorithm to each of our times-series, after removing the best-fitting annual signal and then included the estimated random walk for each component of each station in our velocity solution.

4 RESULTS

Velocity estimates for the Pyrenees region are shown in Fig. 4 in a reference frame defined by minimizing the horizontal velocities of seven stations in Western Europe north of the Pyrenees (Table 1). These seven stations fit our assumed model of no relative motion with a weighted rms of 0.28 mm yr^{-1}. With respect to our western European reference frame, most of the stations south of the Pyrenees move south to south–southwest at ∼0.5–1.5 mm yr^{-1}. As expected from the earthquake focal mechanisms and topography, the stations within the CCR (EBRE, BELL, CASS, GARR and MATA) exhibit a different pattern and will be excluded from our analysis. One of these five stations, MATA, located in Mataró on the Mediterranean coast of Catalonia, moves with 0.58 ± 0.19 mm yr^{-1} velocity in the direction of $205 \pm 20^\circ$. Previous levelling studies of vertical movements by Giménez *et al.* (1996) found anomalous motion (between Caldetes and Arenys points) in the vicinity of the MATA station and related it with tectonic activity. In 1927, an earthquake of VII MSK intensity occurred in the area and several more intensity V earthquakes have been experienced since then (Goula *et al.* 1992). Taking into account all the above evidence (from GPS, levelling and seismicity), we suspect real tectonic deformation in the area of MATA but do not have sufficient station density to characterize the deformation.

We excluded from Fig. 4 two stations (AVEL and PERP Table 1) for which the velocity estimates and uncertainties are large and clearly anomalous and are presumably caused by monument instability or other local motion of non-tectonic origin. In the Supporting Information section we include a map of a larger area with the location and velocities of the reference sites from western Europe. We also include a table of the station information (monumentation, receiver, antenna type and dome) and time-series plots for all the Pyrenees stations.

To assess the strain environment of the central and western region of the Pyrenees, where the seismicity and the focal mechanisms are concentrated, we construct a profile approximately perpendicular to the range and estimate the best-fitting linear slope for 20 stations (excluding SANG, a 2.5σ outlier; Fig. 5). The profile has a scatter about the best-fitting slope with a weighted rms of 0.21 mm yr^{-1} and a normalized rms of 1.12. Scaling the uncertainty of the estimated slope by the nrms gives a velocity gradient of 0.0025 ± 0.0005 mm yr^{-1} km^{-1} or 2.5 ± 0.5 nstrain yr^{-1}. If our error model is correct (see below) the extension rate in the western Pyrenees is significant at >99 per cent confidence. The profile suggests that most of the deformation may be concentrated within a 30 km region between stations ORON and BIAZ, corresponding to the steepest slope of the Pyrenees. If so, the strain rate in this region could be as high as 9 nstrain yr^{-1}.

5 DISCUSSION

5.1 Assessment of uncertainties

We tested our error model in three ways. First we compared the velocities estimated from our 3.5 yr solution for 12 stations in western Europe and northern Africa with the ITRF 2008 velocities determined from GPS observations spanning 10 or more years. For these stations, our velocities matched the ITRF 2008 velocities with χ^2/dof in the horizontal components of ∼1.0 (wrms ∼0.2 mm yr^{-1}). Velocity differences for eight of the 12 stations fall within their 70 per cent confidence ellipses and 11 of 12 within their 95 per cent confidence ellipses.

Second, we used the CATS software of Williams (2008) to estimate velocity uncertainties from the time-series using a model of an annual term, white noise and flicker noise. Of the 12 stations in our Pyrenees profile (Fig. 5) for which the CATS analysis produced a valid estimate of uncertainty in the north component, eight differ from the RS estimate by less than 25 per cent. For ALSA, LNDA, FUEN and LOSA, however, the CATS uncertainties are larger factors of 1.7 to 2.4. These four stations have annual amplitudes of 0.5–1.3 mm and two of them (FUEN, LNDA) are the only stations

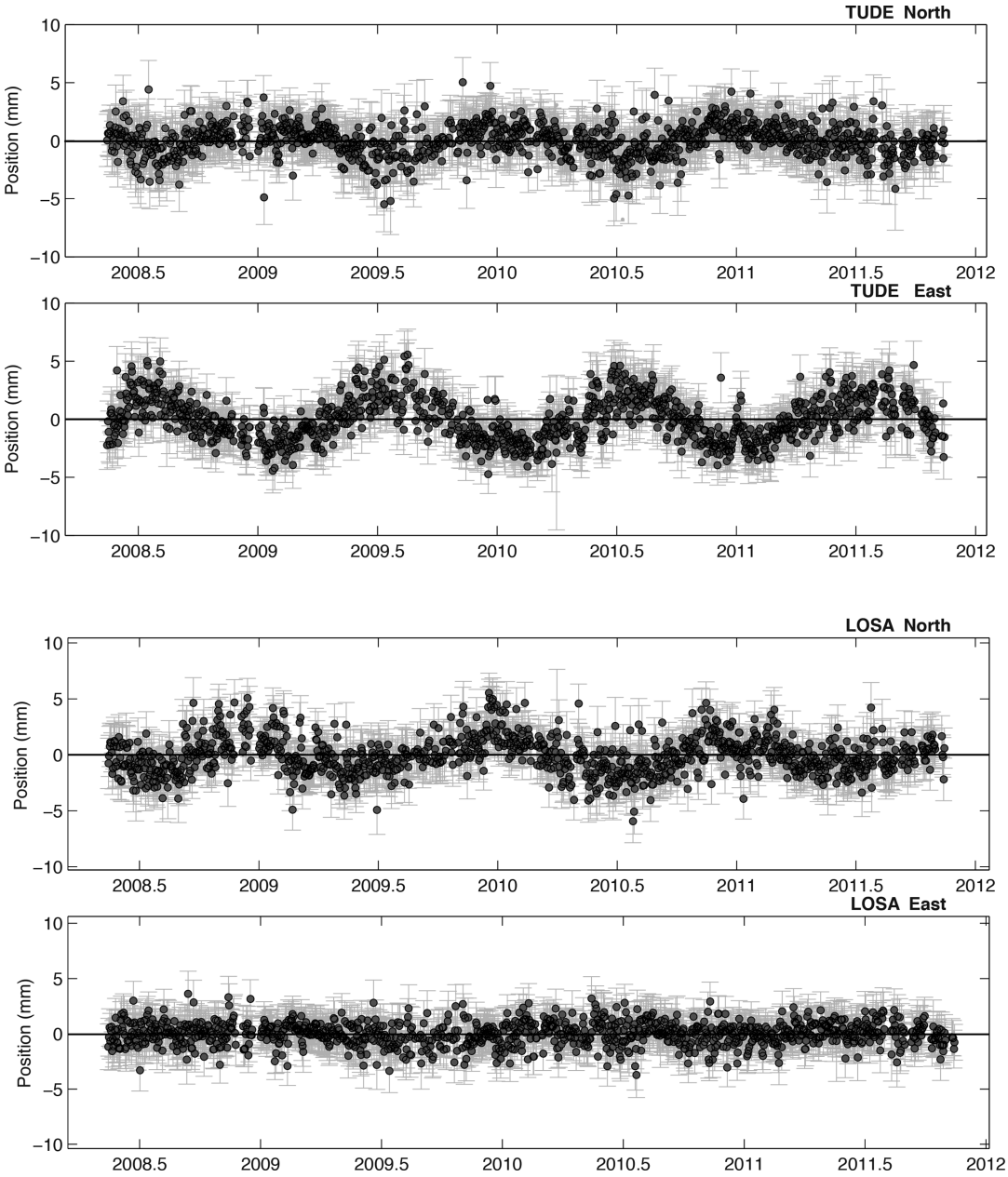

Figure 3. North and East position estimates of TUDE and LOSA stations.

in the profile whose data spans (3.3 yr) fail to match the 3.5 yr that minimizes the effect of annual signatures on the velocity estimates.

Finally, we tested the sensitivity of our strain rate estimates to differing time spans and whether or not we removed an annual term for each station in the analysis. With time spans shorter than 3.5 yr, we found changes in the velocities of some stations in the western region, most critically TUDE and LOSA, as large as 0.5 mm yr^{-1} when the annual term was not removed. However, with the 3.5 yr span, the largest changes are $\sim$0.1 mm yr^{-1}. With the common 3.5-yr data span, whether or not the annual term is removed changes the strain estimate by $\sim$0.1 nstrain yr^{-1}, less than 0.2σ.

5.2 Strain interpretation

The estimated geodetic strain rate in the western part of the Pyrenees, where the instrumental seismicity is mainly concentrated, shows a spatially average rate of extension at $\sim$3 nstrain yr^{-1} perpendicular to the strike of the Pyrenees (roughly NNE–SSW). The direction of extension is consistent with the stress orientation deduced from the focal mechanisms of Stich *et al.* (2006, 2010), as well as, with the strain–stress map calculated by Olaiz *et al.* (2009) and De Vicente *et al.* (2008). The magnitude of the extension, although small, is in agreement with estimates found for example, in the western Alps by Vigny *et al.* (2002) using GPS observations. This finding is also in agreement with previous studies, where the extension are explained by local relaxation processes due to gravitational collapse (Choukroune & Seguret 1973; Rey *et al.* 2001).

5.3 Earthquake recurrence interval

The recurrence time of the MCE (Krinitzsky 2002) that can be expected to occur in a region is related to the rate of strain accumulation and the properties of the crust. Specifically, Kagan

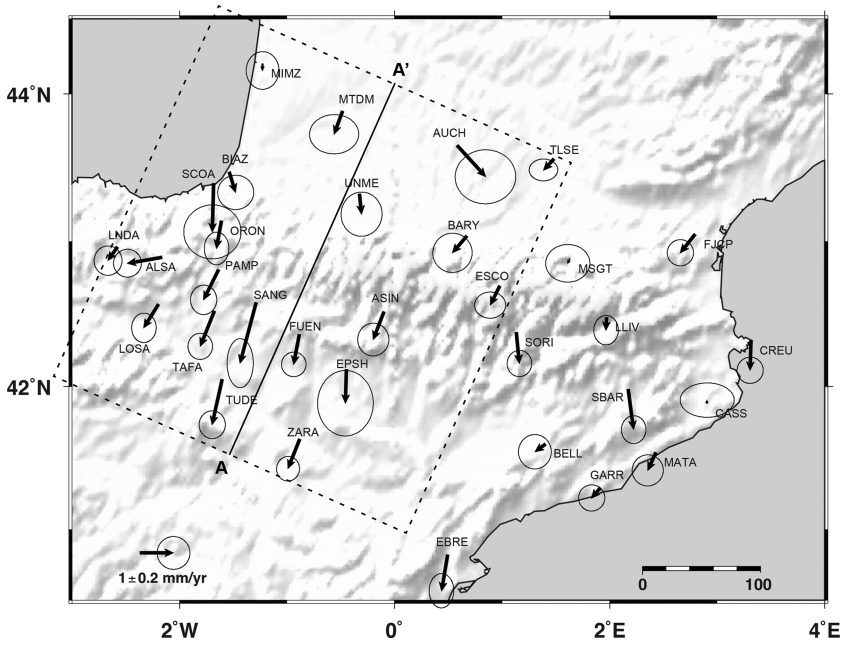

Figure 4. Map of the GPS horizontal velocities of the Pyrenees. The velocities are presented in Eurasia-fixed reference frame with 95 per cent confidence limits. A–A' shows the orientation and stations included in the velocity profile shown in Fig. 5.

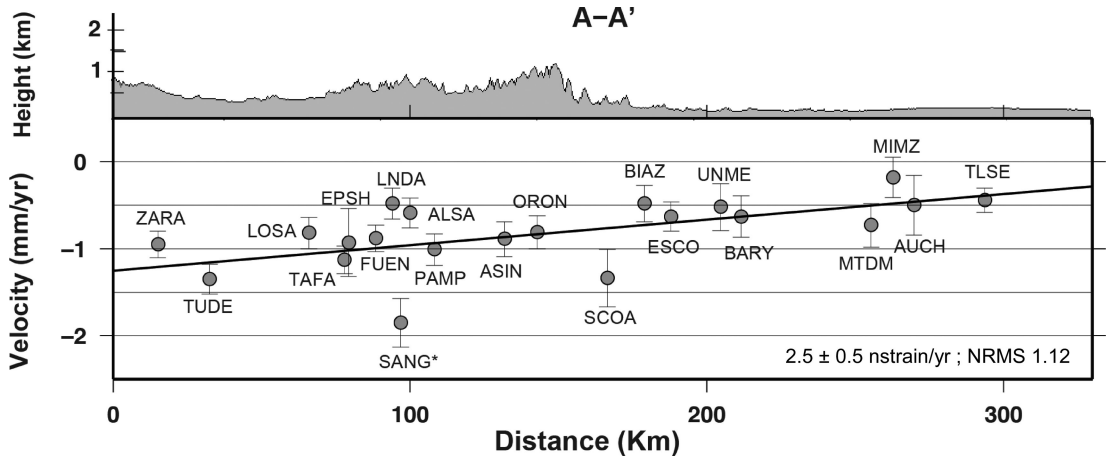

Figure 5. GPS velocities projected onto a N024°E profile, approximately perpendicular to the strike of the Pyrenees in the western and central regions (see Fig. 4). Topography is shown with 16 × vertical exaggeration. Station SANG* is shown but excluded from the estimation of the slope and the statistics.

(2002) gives the recurrence interval T for an earthquake scalar moment M_0

$$T(M_0) = \left[\frac{1}{1-\beta}\right] \frac{M_0^{\beta} M_{\rm cm}^{1-\beta}}{\dot{M}_{\rm g}} \tau(2-\beta)\varepsilon_{\rm m},$$

where $M_{\rm cm}$ is the scalar moment for the MCE, $\beta = \frac{2}{3}b_{\rm value}$, τ is a gamma function and $\varepsilon_{\rm m} = \exp(M_0/M_{\rm cm})$ and $\dot{M}_{\rm g}$ is the geodetic moment rate, given by (Savage & Simpson 1997):

$$\dot{M}_{\rm g} = 2\mu H S \mathrm{Max}\left|\dot{\varepsilon}_1\right|, \left|\dot{\varepsilon}_2\right|, \left|\dot{\varepsilon}_1 + \dot{\varepsilon}_2\right|,$$

where μ is the shear modulus, S represents an area within a geodetic polygon at the Earth's surface and H is the seismogenic depth. For our calculation, we compute both M_0 and $M_{\rm cm}$ from the magnitude of the maximum earthquake in the seismic record for Pyrenees region ($M_{\rm w} = 6.5$; (Olivera *et al.* 1992) using

$$\log M_0 = 1.5 M_{\rm w} + 16$$

(Hanks & Kanamori 1979).

We assume a universal $b_{\rm value}$ of 1 for the Pyrenees (Secanell *et al.* 2008), a shear modulus of 30 GPa and a seismogenic depth of 15 km (Perea 2009). If we use our estimate of the average strain rate (2.7 nstrain yr^{-1}) for the entire region of significant seismicity (160 km × 75 km), we obtain a recurrence time for an $M_{\rm w}$ 6.5 earthquake of ∼2500 yr. If a higher strain rate (9 nstrain yr^{-1}) is valid for the western region of highest seismicity, bounded by stations BIAZ, UNME, ORON and ASIN (100 km × 40 km), then the estimated recurrence interval is ∼2200 yr.

6 CONCLUSIONS

We analysed data from 49 CGPS over a 3.5 yr period to assess deformation rates across and within the Pyrenees. Stations south of the western and central Pyrenees have velocities with respect to western Europe between 0.5 and 1.5 mm yr^{-1} and show a relatively coherent pattern unaffected by modelling assumptions. A profile across this region shows extension perpendicular to the

range at rate of 2.5 ± 0.5 nstrain yr^{-1}. This strain rate is consistent with the stress orientations inferred from earthquake focal mechanisms in the western region (Stich *et al.* 2006, 2010). There is a suggestion of strain rates a factor of three higher for the western area of highest seismicity but station density is insufficient to provide a rigorous estimate. This ongoing deformation implies a recurrence time for the MCE (M_w 6.5) of 2200–2500 yr.

ACKNOWLEDGMENTS

This work is part of Topo-Iberia project (CSD2006–00041) funded by the Spanish Ministry of Science and Innovation. EA was supported by FPU pre-doctoral grant (AP-2008–01482) from the Ministry of Education of Spain, AE by an APIF pre-doctoral grant of University of Barcelona, RK by U.S. National Science Foundation grant EAR-0838488 and IV by Torres Quevedo grant 2008–03-08109 from the Spanish Ministry of Science and Innovation. We are grateful to all the individuals and institutions who contributed to the installation, operation and acquisition of the GPS data throughout the years: ERGPS (IGN, Spain), CATNET (ICC, Catalonia, Spain), RGAN (Navarra Region, Spain), RGP (France), EUREF and IGS. We thank Daniel Stich for providing focal mechanisms from 1986–2008 and Robert Reilinger, Mike Floyd and Thomas Herring for their helpful comments on the manuscript. Most of the figures were prepared using the public domain Generic Mapping Tools GMT (Wessel & Smith 1991).

REFERENCES

Alasset, P.-J. & Meghraoui, M., 2005. Active faulting in the western Pyrénées (France): Paleoseismic evidence for late Holocene ruptures, *Tectonophysics,* **409**(1–4), 39–54, doi:10.1016/j.tecto.2005.08.019.

Altamimi, Z., Collilieux, X. & Métivier, L., 2011. ITRF2008: an improved solution of the international terrestrial reference frame, *J. Geodyn.,* **85**(8), 457–473.

Banda, E. & Santanach, P., 1992. The Valencia trough (western Mediterranean): An overview, *Tectonophysics,* **208**(1–3), 183–202.

Beutler, G., Moore, A. & Mueller, I., 2008. The international global navigation satellite systems service (IGS): development and achievements, *J. Geodyn.,* **83**(3), 297–307, doi:10.1007/s00190-008-0268-z.

Blewitt, G. & Lavallée, D., 2002. Effect of annual signals on geodetic velocity, *J. geophys. Res,* **107**(7), 9–1, doi:10.1029/2001JB000570.

Briais, A., Armijo, R., Winter, T., Tapponnier, P. & Herbecq, A., 1990. Morphological evidence for Quaternary normal faulting and seismic hazard in the eastern Pyrenees, *Ann. Tectonicae,* **4**(1), 19–42.

Bruyninx, C., Becker, M. & Stangl, G., 2001. Regional densification of the IGS in europe using the EUREF permanent GPS network (EPN), *Phys. Chem. Earth Part A,* **26**(6–8), 531–538, doi:10.1016/S1464-1895(01)00096-5.

Caputo, M., Milana, G. & R.J., 1984. Topography and its isostatic compensation as a cause of seismicity of the apennines, *Tectonophysics,* **102**(1–4), 333–342.

Chenel, F. *et al*., 2009. First results of the 2008 RESPYR GPS Campaign in the Pyrenees, *Gephys. Res. Abs.,* 11, 4535.

Choukroune, P. & Seguret, M., 1973. Tectonics of the Pyrenees: role of compression and gravity, in *Gravity and Tectonics,* pp. 141–156, John Wiley and Sons, New York.

Choukroune, P., 1992. Tectonic evolution of the Pyrenees, *Annual Rev. Earth Planet. Sci.,* **20,** 143–158.

De Vicente, G., Cloetingh, S., Munñoz-Martín, A., Olaiz, A., Stich, D., Vegas, R., Galindo-Zaldívar, J. & Fernández-Lozano, J., 2008. Inversion of moment tensor focal mechanisms for active stresses around the microcontinent Iberia: Tectonic implications, *Tectonics,* **27**(TC1009), doi:10.1029/2006TC002093.

Dong, D., Herring, T.A. & King, R.W., 1998. Estimating regional deformation from a combination of space and terrestrial geodetic data, *J. Geodyn.,* **72**(4), 200–214, doi:210.1007/s001900050161.

Duquesnoy, T., 2003. The French GPS Permanent Network, in *Proceedings of the FIG Working Week,* TS5.3.

Fernandes, R.M.S., Miranda, J.M., Meijninger, B.M.L., Bos, M.S., Noomen, R., Bastos, L., Ambrosius, B.A.C. & Riva, R.E.M., 2007. Surface velocity field of the Ibero-Maghrebian segment of the Eurasia-Nubia plate boundary, *Geophys. J. Int.,* **169**(1), 315–324, doi:10.1111/j.1365-246X.2006.03252.x.

Figueras, E. *et al*., 2006. Analysis of the september 2004 seismic crisis in the area of the 1428 earthquake (I_0 = IX), eastern Pyrenees (Spain), in *Proceeding of the First European Conference on Earthquake Engineering and Seismology,* Geneva, Switzerland, 1, 502, paper 268.

Fleta, J., Soro, M., Giménez, J. & Suriñach, E., 1996. Red GPS para medidas geodinámicas en el Pirineo (ResPyr), *Geogaceta,* **20**(4), 992–995.

Fleta, J., Santanach, P., Goula, X., Martinez, P., Grellet, B. & Masana, E., 2001. Preliminary geologic, geomorphologic and geophysical studies for the paleoseismological analysis of the Amer fault (NE Spain), *Neth. J. Geosci.,* **80**(3–4), 243–253.

Gagnepain-Beyneix, J., Haessler, H. & Modiano, T., 1982. The pyrenean earthquake of february 29, 1980: An example of complex faulting, *Tectonophysics,* **85**(3–4), 273–290.

Gallart, J., Daignières, M., Gagnepain-Beyneix, J. & Hirn, A., 1985. Relationship between deep structure and seismicity in the western Pyrenees, *Ann. Geophys,* **3,** 239–248.

Garate, J. *et al*., 2008. Topo-Iberia Project: a new continuous GPS network to monitorize deformations in the South-West European Region, *GeoTemas,* **10,** 1543–1547.

Giménez, J., Suriñach, E., Fleta, J. & Goula, X., 1996. Recent vertical movements from high-precision leveling data in northeast Spain, *Tectonophysics,* **263,** 149–161.

Goula, X., Olivera, C., Escuer, J., Fleta, J., Grellet, B. & Bousquet, J.C., 1992. Neotectonics and seismicity of the area of the seismic crisis of 1427–28 in Catalonia, in *Proceedings of the 22nd General Assembly of the European Seismological Comission,* Barcelona, Spain, pp. 333–338.

Goula, X., Talaya, J., Térmens, A., Colomina, I., Fleta, J., Grellet, B. & Granier, T., 1996. Avaluació de la potencialitat sísmica del Pirineu oriental: primers resultats de les campanyes GPS PotSis'92 i PotSis'94, *Revista Catalana de Geografia,* **11**(28), 41–48.

Goula, X., Olivera, C., Fleta, J., Grellet, B., Lindo, R., Rivera, L.A., Cisternas, A. & Carbon, D., 1999. Present and recent stress regime in the eastern part of the Pyrenees, *Tectonophysics,* **308**(4), 487–502.

Hanks, T.C. & Kanamori, H., 1979. A moment magnitude scale, *J. geophys. Res.,* **84**(B5), 2348–2350.

Herraiz, M. *et al*., 2000. The recent (upper Miocene to Quaternary) and present tectonic stress distributions in the Iberian Peninsula, *Tectonics,* **19**(4), 762–786.

Herring, T., 2003. MATLAB Tools for viewing GPS velocities and time series, *GPS Solut.,* **7**(3), 194–199, doi:10.1007/s10291-003-0068-0.

Herring, T.A., King, R.W. & McClusky, S.C., 2010. *Introduction to GAMIT/GLOBK Release 10.4,* p. 48, Department of Earth, Atmospheric, and Planetary Sciences, Massachusetts Institute of Technology, Cambridge, MA.

Kagan, Y.Y., 2002. Seismic moment distribution revisited: II. moment conservation principle, *Geophys. J. Int.,* **149**(3), 731–754.

Khazaradze, G., Fleta, J., Goula, X., Suriñach, E., Talaya, J. & Térmens, A., 2004. Quantifying crustal deformations with GPS in the eastern Pyrenees, in *12th General Assembly of the WEGENER project "Integrated Modelling of Crustal Deformation",* International Association of Geodesy (IAG), Tangier, Morocco.

Krinitzsky, E.L., 2002. How to obtain earthquake ground motions for engineering design, *Eng. Geol.,* **65**(1), 1–16, doi:10.1016/S0013-7952(01)00098-9.

Masana, E., Villamarín, J.A., Sánchez-Cabañero, J.G., Plaza, J. & Santanach, P., 2001. Seismogenic faulting in an area of low seismic activity: paleoseismicity of the El Camp fault (Northeast Spain), *Neth. J. Geosci.,* **80**(3–4), 229–241.

McClusky, S. *et al*., 2000. Global Positioning System constraints on plate kinematics and dynamics in the eastern Mediterranean and Caucasus, *J. geophys. Res.,* **105**(B3), 5695–5719.

Niemi, N.A., Wernicke, B.P., Friedrich, A.M., Simons, M., Bennett, R.A. & Davis, J.L., 2004. BARGEN continuous GPS data across the eastern Basin and Range Province, and implications for fault system dynamics, *Geophys. J. Int.,* **159**(3), 842–862, doi:10.1111/j.1365-246X.2004.02454.x.

Nocquet, J.M. & Calais, E., 2003. Crustal velocity field of western Europe from permanent GPS array solutions, 1996–2001, *Geophys. J. Int.,* **154**(1), 72–88.

Olaiz, A.J., Muñoz-Martín, A., De Vicente, G., Vegas, R. & Cloetingh, S., 2009. European continuous active tectonic strain–stress map, *Tectonophysics,* **474,** 33–40, doi:10.1016/j.tecto.2008.06.023.

Olivera, C., Susagna, T., Roca, A. & Goula, X., 1992. Seismicity of the Valencia trough and surrounding areas, *Tectonophysics,* **203,** 99–109.

Olivera, C., Redondo, E., Lambert, J., Riera Melis, A. & Roca, A., 2006. Els terratrèmols dels segles XIV i XV a Catalunya, *Monografies,* **30,** 1–407.

Ortuño, M., Queralt, P., Martí, A., Ledo, J., Masana, E., Perea, H. & Santanach, P., 2008. The North Maladeta fault (Spanish Central Pyrenees) as the Vielha 1923 earthquake seismic source: recent activity revealed by geomorphological and geophysical research, *Tectonophysics,* **453,** 246–262, doi:10.1016/j.tecto.2007.06.016.

Perea, H., Figueiredo, P.M., Carner, J., Gambini, S. & Boydell, K., 2003. Paleosismological data froma new trench across the El Camp Fault (Catalan Coastal Ranges, NE Iberian Peninsula), *Ann. Geophys.,* **46**(5), 763–774.

Perea, H., 2009. The Catalan seismic crisis (1427 and 1428; NE Iberian Peninsula): geological sources and earthquake triggering, *J. Geodyn.,* **47,** 259–270, doi:10.1016/j.jog.2009.01.002.

Reilinger, R. *et al*., 2006. GPS constraints on continental deformation in the Africa-Arabia-Eurasia continental collision zone and implications for the dynamics of plate interactions, *J. geophys. Res,* **111**, B05411, doi:10.1029/2005JB004051.

Rey, P., Vanderhaeghe, O. & Teyssier, C., 2001. Gravitational collapse of the continental crust: definition, regimes and modes, *Tectonophysics,* **342**(3–4), 435–449, doi:10.1016/S0040-1951(01)00174-3.

Roca, E., Sans, M., Cabrera, L. & Marzo, M., 1999. Oligocene to Middle Miocene evolution of the central Catalan margin (northwestern Mediterranean), *Tectonophysics,* **315**(1–4), 209–229.

Savage, J.C. & Simpson, R.W., 1997. Surface strain accumulation and the seismic moment tensor, *Bull. seism. Soc. Am.,* **87**(5), 1345–1353.

Secanell, R. *et al*., 2008. Probabilistic seismic hazard assessment of the Pyrenean region, *J. Seism.,* **12,** 323–341.

Serpelloni, E., Vannucci, G., Pondrelli, S., Argnani, A., Casula, G., Anzidei, M., Baldi, P. & Gasperini, P., 2007. Kinematics of the Western Africa-Eurasia plate boundary from focal mechanisms and GPS data, *Geophys. J. Int.,* **169**(3), 1180–1200, doi:10.1111/j.1365-246X.2007.03367.x.

Shen, Z.-K., King, R.W., Agnew, D.C., Wang, M., Herring, T.A., Dong, D. & Fang, P., 2011. A unified analysis of crustal motion in Southern California, 1970–2004: The SCEC crustal motion map, *J. geophys. Res.,* **116,** B11402, doi:10.1029/2011JB008549.

Souriau, A. & Pauchet, H., 1998. A new synthesis of Pyrenean seismicity and its tectonic implications, *Tectonophysics,* **290,** 221–244.

Stich, D., Serpelloni, E., Mancilla, F. & Morales, J., 2006. Kinematics of the Iberia-Maghreb plate contact from seismic moment tensors and GPS observations, *Tectonophysics,* **426**(3–4), 295–317, doi:10.1016/j.tecto.2006.08.004.

Stich, D., Martín, R. & Morales, J., 2010. Moment tensor inversion for Iberia-Maghreb earthquakes 2005–2008, *Tectonophysics,* **483**(3–4), 390–398.

Sylvander, M., Souriau, A., Rigo, A., Tocheport, A., Toutain, J.P., Ponsolles, C. & Benahmed, S., 2008. The 2006 November, ML = 5.0 earthquake near Lourdes (France): new evidence for NS extension across the Pyrenees, *Geophys. J. Int.,* **175,** 649–664, doi:10.1111/j.1365-246X.2008.03911.x.

Talaya, J., Feigl, K., Termens, A. & Colomina, I., 1999. Practical lessons from analysis of a GPS network designed to detect movements of ∼1mm/year in the Eastern Pyrenees, *Phys. Chem. Earth.,* **24**(4), 355–359.

Talaya, J., Bosch, E., Ortiz, M. & Parareda, C., 2000. CATNET: a permanent GPS network with real-time capabilities, *Asemblea Hispano Portuguesa de Geodesia y Geofisica,* **2,** 2.

Teixell, A., 1996. The Ansó transect of the southern Pyrenees: basement and cover thrust geometries, *J. geol. Soc. Lond.,* **153,** 301–310.

Térmens, A., Castellote, M., Soro, M., Fleta, J., Goula, X. & Talaya, J., 2000. PotSis'99, PotSis'94 and PotSis'99 GPS campaigns to improve the knowledge of seismic potentiality in the Eastern Pyrenees, *X General Assembly of the WEGENER Project,* WEGENER 2000.

Vergés, J., Fernàndez, M. & Martínez, A., 2002. The Pyrenean orogen: pre-, syn-, and post-collisional evolution, *J. Virtual Explor.,* **8,** 57–76.

Vigny, C. *et al*., 2002. GPS network monitors the Western Alps' deformation over a five-year period: 1993–1998, *J. Geod.,* **76**(2), 63–76, doi:10.1007/s00190-001-0231-8.

Wessel, P. & Smith, W.H.F., 1991. Free software helps map and display data, *EOS, Trans. Am. geophys. Un.,* **72**(41), 441, doi:10.1029/90EO00319.

Williams, S., Bock, Y., Fang, P., Jamason, P., Nikolaidis, R.M., Prawirodirdjo, L., Miller, M. & Johnson, D.J., 2004. Error analysis of continuous GPS position time series, *J. geophys. Res.,* **109**(B03412), doi:10.1029/2003JB002741.

Williams, S., 2008. CATS: GPS coordinate time series analysis software, *GPS Solut.,* **12**(2), 147–153, doi:10.1007/s10291-007-0086-4.

SUPPORTING INFORMATION

Additional Supporting Information may be found in the online version of this article:

Figure S1(a–d). North and East position estimates of 35 CGPS stations located in the Pyrenees.

Figure S2. Regional map including CGPS stations from Europe and Africa. Velocities are in the Western Europe reference frame.

Table S1. Description of processed GPS stations.

Please note: Wiley-Blackwell are not responsible for the content or functionality of any supporting materials supplied by the authors. Any queries (other than missing material) should be directed to the corresponding author for the article.